Alexandria Engineering Journal (2016) 55, 2375–2389

HOSTED BY

Alexandria University

Alexandria Engineering Journal

www.elsevier.com/locate/aej
www.sciencedirect.com

ORIGINAL ARTICLE

47nm alumina–water nanofluid flow within boundary layer formed on upper horizontal surface of paraboloid of revolution in the presence of quartic autocatalysis chemical reaction

Isaac Lare Animasaun *

Department of Mathematical Sciences, Federal University of Technology, Akure, Ondo State, Nigeria

Received 5 March 2016; revised 14 April 2016; accepted 21 April 2016
Available online 24 May 2016

KEYWORDS

Quartic autocatalysis;
Nanofluid;
Gyrotactic microorganisms;
Paraboloid of revolution;
Volume fraction;
Buoyancy induced model

Abstract In this article, a modified version of buoyancy-induced model is considered to investigate the flow of 47nm alumina–water nanofluid along an upper surface of horizontal paraboloid of revolution in the presence of nonlinear thermal radiation, Lorentz force and quartic autocatalysis kind of homogeneous heterogeneous chemical reaction. The case of unequal diffusion coefficients of reactant A (bulk fluid) and B (high concentration of catalyst at the surface) in the presence of bioconvection is considered. Governing equation suitable to unravel the thermophoresis which takes place within the boundary layer is presented. Since chemical reactant B is of higher concentration at the surface more than the concept described as cubic autocatalytic, the suitable schemes are herein described as isothermal quartic autocatalytic reaction and first order reaction. The viscosity and thermal conductivity are assumed to vary with volume fraction (ϕ) and suitable models for the case $0\% \leqslant \phi \leqslant 0.8\%$ are adopted. The transformed governing equations are solved numerically using Runge–Kutta fourth order along with shooting technique (RK4SM). Good agreement is obtained between the solutions of RK4SM and MATLAB `bvp5c` for a limiting case. The influence of some pertinent parameters on velocity, temperature, diffusion of motile microorganism, concentration of bulk fluid and catalyst is illustrated graphically and discussed.

1. Introduction

Aerosol can be described as a suspension of fine liquid droplets or solid particles in air or liquid. Practically speaking, small particle(s) can be driven from a hot surface towards a cold surface. For instance, small particles (e.g. dry dust) when suspended in a gas (e.g. air) with a temperature gradient, experience a force in the direction of the temperature gradient

* Tel.: +234 8034117546.
E-mail addresses: anizakph2007@gmail.com, ilanimasaun@futa.edu.ng
Peer review under responsibility of Faculty of Engineering, Alexandria University.

http://dx.doi.org/10.1016/j.aej.2016.04.030

(migrate towards the direction of decreasing temperature). In this situation, the velocity of such particle(s) which drives it from the region of hot surface to the region of cold surface is called thermophoretic velocity. The force experienced by the suspended particle(s) due to the temperature gradient is called thermophoretic force. This concept was first observed and reported by John Tyndall (Physicist/Chemist from Ireland) in the year 1870. Thereafter, John William Strutt (3rd Baron Rayleigh) explained this report in such a way that scientists deeply understood the contribution of John Tyndall; see Davis [1]. A common example of the phenomenon is the blackening of the glass globe of a kerosene lantern; the temperature gradient established between the flame and the globe drives the carbon particles produced in the combustion process towards the globe where they deposit; Talbot et al. [2]. Another occurrence of thermophoresis can be found at the edge of fluorescent bulb. According to Tsai et al. [3] on combined effects of thermophoresis and electrophoresis on particle deposition onto a thin slice of semiconductor material used in electronic for fabrication of integrated circuits; the deposition mechanisms for particles include Brownian diffusion, convection, thermophoresis and electrophoresis. Thermophoresis is of practical importance in many industrial applications, such as in aerosol collection (thermal precipitator), micro contamination control, removing small particles from gas streams, nuclear reactor safety, in studying the particulate material deposition on turbine blades, and also in determining exhaust gas particle trajectories from combustion devices. Animasaun [4] reported the dynamics of unsteady magnetohydrodynamic fluid flow with thermophoresis of particles past a vertical porous plate moving through a binary mixture in an optically thin environment. Sandeep et al. [5] deliberated on boundary layer flow of a thermophoretic MHD dissipative nanofluid over an unsteady stretching sheet in a porous medium.

Nanoparticles can be described as particles between 1nm and 100nm in size. Nanoparticle research is currently an area of intense scientific interest due to a wide variety of potential applications in engineering and biomedical. When nanoparticles are controllably dispersed in base fluid, it enhances the properties of the so-called multi-component fluid or two-phase fluid. The term "*nanofluid*" was proposed by Choi [6], referring to dispersions of nanoparticles in the base fluid such as water. Nguyen et al. [7] reported that sedimentation, shear stress and agglomeration are few problems that can be referred to as an agent which may limit the mixtures of nanoparticles in a nanofluid. Sandeep et al. [8] reported stagnation point flow, heat and mass transfer behavior of MHD Jeffrey nanofluid in the presence of induced magnetic field. The word "*Bioconvection*" was first introduced in the report of James Henry Platt with the aim to call the attention of other researchers to the physics of streaming patterns observed in dense cultures of free-swimming organisms. According to Platt [9], the moving polygonal patterns in dense cultures of *Tetrahymena* and other *ciliates* and *flagellates* look like "Benard cells" but are not due to thermal convection. There exist many bacteria (organisms) and it is a well-known fact that many bacteria can be damaged and sometimes killed if exposed to high temperature. In contrary, thermophile is an organism commonly found in various heated regions of the earth. Ghorai and Hill [10] further explained that bioconvection is the term used to describe the phenomenon of spontaneous pattern formation in suspensions of microorganisms such as bacteria and algae. Bioconvection can now be described as the macroscopic convective motion of fluid caused by density gradient and is created by collective swimming of motile microorganisms. Like natural convection, bioconvection is caused by unstable density stratification. Kuznetsov and Avramenko [11] explained that if bioconvection develops, it enhances mixing and slows down the settling of the particles which may be of importance in pharmaceutical applications. Khan and Makinde [12] investigated nanofluid bioconvection due to gyrotactic microorganisms and remarked that these self-propelled motile microorganisms may increase the density of the base fluid by swimming in a particular direction, thus causing bioconvection. For more related contributions on heterogenous mixed convection of alumina/water nanofluid, nanofluid flow inside porous micro-channel in the presence and absence of heat source/sink, heat convection inside concentric annulus filled with alumina–water nanofluid and unsteady motion of vertically falling spherical particles see Refs. [13–17]. Recently, Raees et al. [18] reported that bioconvection in nanofluids has great potential in Colibri microvolumes spectrometer and also to improve the stability of nanofluids.

Chemical reaction can be explained as an interaction between two or more chemicals which produces either one or more new chemical compounds. An example is nth order of chemical reaction which may not require catalyst. Animasaun [19] analyzed such effects in MHD dissipative Casson fluid flow in the presence of thermophoresis. Many chemical reactions actually require heat and accelerator (i.e. catalyst). A chemical reaction in which catalyst is in the same phase (i.e. in the same state of matter) as the reactant(s) is known as homogeneous catalytic reaction. Reactions between two gases and between two liquids are typical examples of homogeneous catalytic reactions. Another example is the mixture of household cooking gas with oxygen gas leading to flame. In heterogeneous catalytic reaction, catalyst and reactants are in different phases (i.e. different states of matter). Examples of heterogeneous catalytic reactions are chemical reactions between gas & liquid, gas & solid and liquid & solid. In addition to this example, a chemical reaction in which one or more reactants undergo chemical change at an interface (i.e. on the surface of a solid catalyst) is called heterogeneous catalytic reaction. When fluid moves along a surface, a thin layer is formed in the vicinity of a surface bounding the fluid; Ludwig Prandtl called it "*boundary layer*". Chaudhary and Merkin [20] introduced a simple model for homogeneous heterogeneous reactions in stagnation-point boundary-layer flow in which the homogeneous (bulk) reaction is assumed to be given by isothermal cubic autocatalator kinetics and the heterogeneous (surface) reaction by first order kinetics. Scott [21] considered quadratic and cubic autocatalytic together with rates of their chemical reaction; then coupled the equation with the diffusion of the reactants through a permeable boundary from an external reservoir where the concentrations are held constant. Motsa et al. [22] investigated the case of equal diffusion coefficients of chemical species A and B in the stagnation point nanofluid flow in the presence of homogeneous heterogeneous reactions using successive linearization method (SLM). Sandeep et al. [23] explained the effects of induced magnetic field on cubic autocatalytic reaction which often occurs in viscoelastic fluid flows toward a stagnation point. In most cases when the concentration of homogeneous species B is highly substantial, the cubic autocatalator kinetics may not be sufficient;

hence isothermal quartic autocatalytic reaction is needed in order to unravel the motion and behavior of the flow within boundary layer.

Variable thickness is one of the significant properties of an object. In the industry, there are many surfaces in which its thickness is not uniform and fluid flows over it. To a reasonable extent, the upper half surface of an horizontal object with variable thickness can be described as paraboloid of revolution. Thin needle is a typical example of slender object (i.e. object with non-uniform thickness). Lee [24] presented boundary layer equation governing the motion of an incompressible fluid flow over a thin needle. Davies and Werle [25] deliberated on the numerical solutions of Navier–Stokes equations for flow past a paraboloid of revolution. Anjali Devi and Prakash [26] numerically investigated the influence of temperature dependent viscosity and thermal conductivity on magnetohydrodynamic flow over stretching sheet with variable thickness. In the research conducted by Fang et al. [27] on boundary layer flow over a continuously stretching sheet with variable thickness, it was reported that for $-0.5 < m < \infty$; a unique solution exists for any given values of the wall thickness parameter. In all the literatures mentioned above, it is worth noticing that various researchers have investigated the flow of nanofluid along horizontal, vertical and inclined surfaces with uniform thickness but there exists no report on boundary layer analysis of nanofluid flow containing both spherical nanoparticles and gyrotactic microorganism over upper horizontal surface of paraboloid of revolution in the presence of quartic autocatalytic kind of homogeneous heterogeneous chemical reaction. Moreover, in the industry, this kind of chemical reaction often occurs within the boundary layer formed on the surface in nanofluid flow. In addition, various researchers have investigated nanofluid flow along horizontal surface with no investigation on the dynamics of nanofluid in the presence of gyrotactic microorganism for higher volume fractions of particles in the flow of 47nm alumina–water nanofluid. In many published articles on the analysis of boundary layer formed in the flow of nanofluid past a surface, viscosity and thermal conductivity of nanofluid have been assumed to be a constant function of volume fraction; this may not be sufficient enough to accurately model the flow due to the fact that these thermo-physical properties vary with volume fraction. For limited case $0\% \leqslant \phi \leqslant 0.02\%$, some researchers has reported the case in which the viscosity varies with volume fraction. All these assumptions and cases that have been published are not suitable to model the case in which the volume fraction relatively falls within the interval $0.02\% \leqslant \phi \leqslant 0.8\%$; hence suitable models are considered in this study. It is paramount to remark that this contribution to the body of knowledge will enhance efficiency and productivity in the industry. Also, it will help engineers to further understand the problem of low thermal conductivity in nanofluid and slow motion in the production of efficient heat transfer liquids.

2. Description of the boundary layer flow and formulation of governing equation

The mathematical formulation which models the boundary layer flow of 47nm alumina–water nanofluid over a surface that can be described as upper paraboloid of revolution in the presence of space dependent internal heat source and nonlinear thermal radiation is investigated. It is assumed that quartic autocatalytic chemical reaction with catalyst decay between reactants A and B occurs as the steady two-dimensional nanofluid flows. The chemical reaction can be furthered described as a kind in which the homogeneous (bulk fluid) reaction with heterogeneous (high concentration of catalyst at the surface) occurs by isothermal quartic autocatalator kinetics and first order kinetics respectively. The nanofluid flow under consideration is assumed to occupy the domain $A(x+b)^{\frac{1-m}{2}} \leqslant y < \infty$ as shown in Fig. 1. However, y minimum could be verified by plotting the graph of $y = A(x+b)^{\frac{1-m}{2}}$ against x using $b = 1$ and $m < 1$ (i.e. $= 0.25$). The immediate fluid layers on the surface are stretched parallel with velocity $U_w = U_o(x+b)^m$. The object herein described as paraboloid of revolution is assumed to be non-porous and non-melting. In this case, x-axis is taken along the direction of the horizontal surface and y-axis is normal to it. The origin of x-axis and y-axis is not the starting point of the flow. Hence, the starting point of the flow at the slot is a function $y = A(x+b)^{\frac{1-m}{2}}$. Consequently, the velocity along x-direction, velocity along y-direction, temperature, concentration of reactant A, concentration of reactant B and density of motile microorganisms at the surface are $u(x,y)$, $v(x,y)$, $T(x,y)$, $a(x,y)$, $\ell(x,y)$ and $N(x,y)$ respectively. As shown in Fig. 1, the temperature of the horizontal surface with variable thickness is of the form $T_w = A(x+b)^{\frac{1-m}{2}}$; here parameter "$m$" is known as velocity power index and "b" is known as parameter related to stretching sheet. Meanwhile, the temperature at free stream is a constant function of temperature. It is assumed that 47nm alumina–water nanofluid is diluted so that the bioconvection instability can be avoided. It is also assumed that the spherical nanoparticles are suspended in the nanofluid using surfactant and hence, prevent nanoparticles from agglomeration. The microorganisms are assumed to have constant distributions on the surface. It is worth mentioning that the base fluid is water so that the gyrotactic microorganisms can survive. In this study, it is also assumed that the existence of spherical nanoparticles has few effects on the motion of the microorganisms. Following the idea and mathematical formulation stated in Kuznetsov and Nield [28,29] and Raees et al. [18] the flux of microorganisms through the boundaries is equal to zero. Mathematically, this can be expressed as

$$\nabla * j = 0. \tag{1}$$

Adopting the concept of homogeneous heterogeneous reaction model proposed by Chaudhary and Merkin [20] and Lynch [30], isothermal quartic autocatalytic reaction within the boundary layer when chemical reactant B is of high concentration at the surface is presented as

$$A + 3B \rightarrow 4B, \tag{2}$$

rate of chemical reaction $= k_1 a\ell^3$ and on the upper horizontal surface of paraboloid of revolution in the presence of catalyst, there exists single isothermal first order reaction of the form

$$A \rightarrow B, \tag{3}$$

rate of chemical reaction $= k_s a$ where "a" and "ℓ" are the concentrations of reactant A and reactant B. Here, k_1 and k_s are known as the reaction rate coefficients which may not be actually referred to as a constant because it includes all the likely parameters that may affect reaction rate except concentration

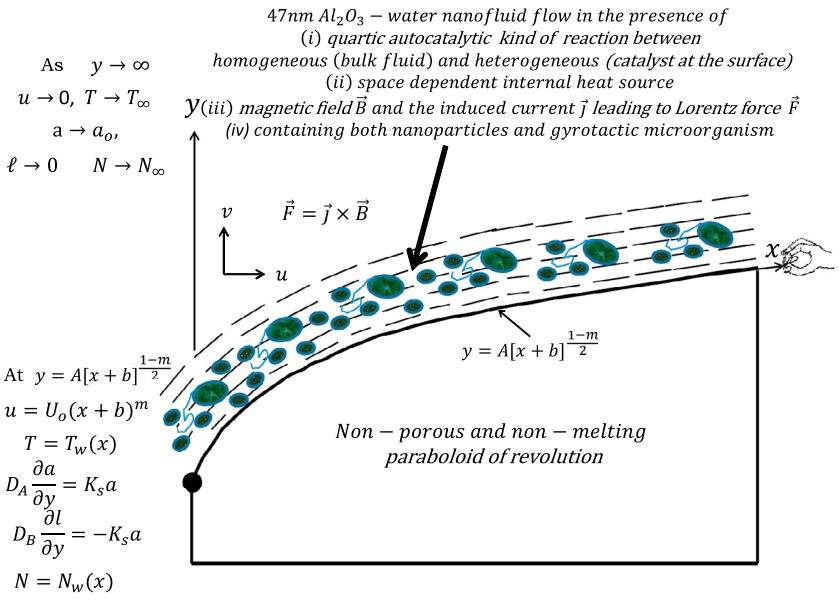

Figure 1 The coordinate system of nanofluid flow past upper horizontal surface of paraboloid of revolution.

which we have explicitly accounted for in Eqs. (2) and (3). Following Pedle et al. [31] and Kuznetsov [32], it is assumed that the random component of microorganisms (gyrotactic) motion in the nanofluid can be approximated by a diffusion process/-concentration in the bulk fluid; hence concentration of the homogeneous chemical reactant A is considered as

$$j = N\upsilon + N\widetilde{\upsilon} - D_m \nabla N,\ \widetilde{\upsilon} = \left(\frac{c_h W_c}{\triangle a}\right)\nabla a. \tag{4}$$

where υ is the velocity vector of the flow, u and v are the velocity components in the x- and y-directions respectively, $\widetilde{\upsilon}$ is the average swimming velocity vector of oxytactic microorganisms, c_h is the chemotaxis constant, W_c is the maximum cell swimming speed and D_m is the diffusivity of microorganisms. Considering a magnetic field $(\overrightarrow{B})$ is applied perpendicular to the flow of an electrically conducting fluid with velocity vector $(\overrightarrow{V})$ in the x direction. Following the illustrations of Anjali Devi and Prakash [26] the interaction of magnetic field $(\overrightarrow{B})$ with the induced current $(\overrightarrow{j})$ and the Lorentz force $(\overrightarrow{F})$ is of the form

$$\overrightarrow{F} = \overrightarrow{j} \times \overrightarrow{B} = \sigma[B(x)]^2 u. \tag{5}$$

2.1. Buoyancy-induced model for fluid flow past a surface that can be described as upper horizontal surface of paraboloid of revolution

According to the report of Joseph Valentin in the year 1987, if ρ_∞ denotes the density of the fluid at the free stream then temperature is T_∞. For temperature difference between the wall (T_w) and free stream layer (T_∞); the density model is presented as

$$\rho = \rho_\infty[1 - \beta(T - T_\infty)] \quad where \quad T_w > T_\infty. \tag{6}$$

Here β is known as the coefficient of volume expansion. Considering moderate variation in temperature, this often leads to negligible change in density

$$\begin{aligned} \delta\rho &= |\rho - \rho_\infty| \\ \delta\rho &= |\rho_\infty[1 - \beta(T - T_\infty)] - \rho_\infty| \\ \delta\rho &= |-\rho_\infty\beta(T - T_\infty)| \\ \delta\rho &= \rho_\infty\beta(T - T_\infty) \end{aligned} \tag{7}$$

For more details on this, see Boussinesq [33]. The buoyancy term

$$\begin{aligned} &g(\rho - \rho_\infty) \approx g\delta\rho \ \ or \\ &g(\rho - \rho_\infty)Cos(\alpha) \approx g\delta\rho \end{aligned} \tag{8}$$

is of the same order of magnitude as the inertia term or the viscous term; so it is not negligible when formulating the buoyancy model suitable to describe fluid flow over a vertical surface with uniform thickness or inclined surface with uniform thickness where α is known as the angle of inclination. Upon equating the approximation in Eq. (8) to Eq. (7), the buoyancy term can be simplified as

$$\begin{aligned} &g(\rho - \rho_\infty) = g\beta\rho_\infty(T - T_\infty),\ \ or \\ &g(\rho - \rho_\infty)Cos(\alpha) = g\beta\rho_\infty(T - T_\infty)Cos(\alpha). \end{aligned} \tag{9}$$

For free convection over a vertical surface with uniform thickness or inclined surface with uniform thickness, the body force term (buoyancy force) and pressure gradient term is algebraically incorporated into the momentum equation as

$$\begin{aligned} &-\frac{\partial p}{\partial x} + \rho g_x = 0 + g\beta\rho_\infty(T - T_\infty),\ \ or \\ &-\frac{\partial p}{\partial x} + \rho g_x = 0 + g\beta\rho_\infty(T - T_\infty)Cos(\alpha). \end{aligned} \tag{10}$$

Here, the pressure gradient term is zero (i.e. $\frac{\partial p}{\partial x} = 0$). It is known that the forced convection requires excessive stretching of some layers of the fluid; this might either be layers of fluid situated at the free stream or fluid layers adjacent to the wall/-surface. For forced convection along a vertical surface with uniform thickness or inclined surface with uniform thickness, the body force term (buoyancy force) and pressure gradient term are algebraically incorporated into the momentum equation as

$$-\frac{\partial p}{\partial x}+\rho g_x = u_\infty \frac{du_\infty}{dx}+0. \tag{11}$$

Here, $\rho g_x = 0$. Also, for mixed convection along a vertical surface with uniform thickness or inclined surface with uniform thickness, the body force term (buoyancy force) together with pressure gradient term are algebraically incorporated into the momentum equation as

$$\begin{aligned} &-\frac{\partial p}{\partial x}+\rho g_x = u_\infty \frac{du_\infty}{dx}+g\beta\rho_\infty(T-T_\infty)\ or\\ &-\frac{\partial p}{\partial x}+\rho g_x = u_\infty \frac{du_\infty}{dx}+g\beta\rho_\infty(T-T_\infty)Cos(\alpha). \end{aligned} \tag{12}$$

This theory is known as Boussinesq approximation which states that density differences are sufficiently small to be neglected, except where they appear in terms multiplied by g (the acceleration due to gravity) see Boussinesq [33]. The essence of the Boussinesq approximation is that the difference in inertia is negligible but gravity is sufficiently strong to make the specific weight appreciably different between any two layers of fluids. This theory was used successfully to investigate typical incompressible temperature dependent fluid viscosity and thermal conductivity in the presence of linear thermal radiation with heat and mass transfer over a vertical surface; see Ref. [34]. Within past few years, modification of theory or model has been something researchers in the field of boundary layer analysis together with heat and mass transfer embrace and investigate in order to test the validity as presented in academic discourse. In order to demonstrate the effects of temperature dependent physical properties for natural convection in a concentric annulus, a modified Boussinesq approximation was developed and used successfully by Shahraki [35]. Diaz et al. [36] reported that in the Boussinesq approximation the main coupling term is the generation of momentum due to temperature gradients together with viscous heating (heat production due to internal friction). For proper and correct analysis of fluid flow along vertical surface with a temperature lesser than that of the free stream (i.e. $T_w < T_\infty$), Boussinesq approximation model was modified and discussed explicitly by Animasaun [37]. It is important to recall that $T_w > T_\infty$ in this case of fluid flow over upper horizontal of paraboloid of revolution as shown in Fig. 1; this calls for modification in order to avoid misleading effect of Grashof number G_{rm}. Also, it may not be valid to investigate fluid flow along a surface which is neither vertical nor inclined as in the case of $m < 1$. In this study, the modified version for free convection and heat transfer suitable to investigate the boundary layer flow is presented as

$$-\frac{\partial p}{\partial x}+\rho g_x = \frac{\partial}{\partial x}\left(g\beta x\frac{m+1}{2}\right)(T-T_\infty)+0. \tag{13}$$

It is assumed that the difference between number density of motile microorganisms in nanofluid N and ambient concentration of microorganism $[\rho_m - \rho_f]$ is constant and not equal to zero. This explains the absence of the term $\frac{\partial}{\partial x}\left(g\omega[\rho_m-\rho_f]x^{\frac{m+1}{2}}\right)(N-N_\infty)$ in Eq. (13).

2.2. Governing equation

Following the formulation of Chaudhary and Merkin [20], the governing boundary-layer equations are of the following form:

$$\frac{\partial u}{\partial x}+\frac{\partial v}{\partial y}=0, \tag{14}$$

$$u\frac{\partial u}{\partial x}+v\frac{\partial u}{\partial y}=\frac{\mu_{nf}}{\rho_{nf}}\frac{\partial^2 u}{\partial y^2}+\frac{\partial}{\partial x}\left(g\beta x\frac{m+1}{2}\right)(T-T_\infty)-\frac{\sigma[B(x)]^2}{\rho_{nf}}u, \tag{15}$$

where the magnetic field $B(x) = B_o(x+b)^{\frac{m-1}{2}}$. Using the idea of Rosseland [38], the energy equation in which nonlinear thermal radiation, thermophoresis and space dependent internal heat source are accounted for is of the form

$$\begin{aligned} u\frac{\partial T}{\partial x}+v\frac{\partial T}{\partial y} &= \frac{\kappa_{nf}}{(\rho Cp)_{nf}}\frac{\partial^2 T}{\partial y^2}-\frac{1}{(\rho Cp)_{nf}}\frac{\partial q_r}{\partial y}\\ &+\tau\left[D_A\frac{\partial a}{\partial y}\frac{\partial T}{\partial y}+\frac{D_T}{T_\infty}\left(\frac{\partial T}{\partial y}\right)^2\right]+\frac{Q_o[T_w(x)-T_\infty]}{(\rho C_p)_{nf}}\\ &\times Exp\left[-ny\sqrt{\frac{m+1}{2}}\sqrt{\frac{U_o}{\vartheta_{bf}}}(x+b)^{\frac{m-1}{2}}\right]. \end{aligned} \tag{16}$$

The Rosseland approximation which is a simplification of the radiative transport equation (RTE) for the case of optically thick media is adopted to account for the radiative heat flux in the nanofluid as

$$q_r = -\frac{4\sigma^*}{3k^*}\frac{\partial}{\partial y}(T\times T\times T\times T), \tag{17}$$

where σ^* and k^* are the Stefan–Boltzmann constant and the mean absorption coefficient respectively. In this case of nanofluid, herein (optically thick) the thermal radiation travels only a short distance before being scattered or absorbed. Eq. (17) introduces a new diffusion term into the energy transport equation which was developed based on the theory of conservation of energy. In this study, it is assumed that the temperature differences within the flow are not sufficiently small. In view of this, it may not be realistic to simplify the radiative heat flux by expanding T^4 in a Taylor series expansion about T_∞ then neglecting higher order terms. Implicit differentiation may be adopted to simplify Eq. (17) and then substitute into Eq. (16). Following the formulation of space dependent internal heat source in Ref. [39], the modified energy equation is now

$$\begin{aligned} u\frac{\partial T}{\partial x}+v\frac{\partial T}{\partial y} &= \frac{\kappa_{nf}}{(\rho Cp)_{nf}}\frac{\partial^2 T}{\partial y^2}+\frac{1}{(\rho Cp)_{nf}}\frac{\partial}{\partial y}\left(\frac{4\sigma^*}{3k^*}4T^3\frac{\partial T}{\partial y}\right)\\ &+\tau\left[D_A\frac{\partial a}{\partial y}\frac{\partial T}{\partial y}+\frac{D_T}{T_\infty}\left(\frac{\partial T}{\partial y}\right)^2\right]+\frac{Q_o[T_w(x)-T_\infty]}{(\rho C_p)_{nf}}\\ &\times Exp\left[-ny\sqrt{\frac{m+1}{2}}\sqrt{\frac{U_o}{\vartheta_{bf}}}(x+b)^{\frac{m-1}{2}}\right]. \end{aligned} \tag{18}$$

Considering the influence of thermophoresis, homogeneous heterogeneous reaction model for the concentrations of reactants A and B, as stated in the reaction scheme Eqs. (2) and (3) is formulated as

$$u\frac{\partial a}{\partial x}+v\frac{\partial a}{\partial y}=D_A\frac{\partial^2 a}{\partial y^2}-K_1 a\ell^3-\frac{D_T}{T_\infty}\frac{\partial^2 T}{\partial y^2}, \tag{19}$$

$$u\frac{\partial \ell}{\partial x}+v\frac{\partial \ell}{\partial y}=D_B\frac{\partial^2 \ell}{\partial y^2}+K_1 a\ell^3+\frac{D_T}{T_\infty}\frac{\partial^2 T}{\partial y^2}, \tag{20}$$

Based on the fact that reactant A and reactant B undergo chemical changes at an interface, the heterogeneous catalytic reaction is properly accounted for in the boundary condition. Following the idea of Ref. [18], the governing equation for dimensional motile microorganism in homogeneous bulk fluid is

$$u\frac{\partial N}{\partial x}+v\frac{\partial N}{\partial y}+\frac{\partial}{\partial y}\left(N\frac{c_h W_c}{\Delta a}\frac{\partial a}{\partial y}\right)=D_n\frac{\partial^2 N}{\partial y^2}. \tag{21}$$

Suitable boundary conditions governing the flow along upper horizontal surface of paraboloid of revolution are

$$u=U_o(x+b)^m,\ v=0,\ T=T_w,\ D_A\frac{\partial a}{\partial y}=K_s a,\ D_B\frac{\partial \ell}{\partial y}$$
$$=-K_s a,\ N=N_w\ at\ y=A(x+b)^{\frac{1-m}{2}}. \tag{22}$$

$$u\to 0,\ T\to T_\infty,\ a\to a_o,\ \ell\to 0,\ N\to N_\infty\ as\ y\to\infty. \tag{23}$$

2.3. Variation in relative viscosity and thermal conductivity of nanofluid with volume fraction of spherical particles

There exist some theoretical and experimental models which estimate particle suspension viscosity of a nanofluid. Nanofluid has some common features with solid–fluid mixtures. The Einstein' formulae is of the form

$$\frac{\mu_{nf}}{\mu_{bf}}=1+2.5\phi. \tag{24}$$

Comparison of Eq. (24) with experimental result has shown that Einstein' formula adequately describes the viscosity of suspensions at volume concentrations of particles $\phi\leqslant 0.02$; see Rudyak [40]. It is worth mentioning that model Eq. (24) is only suitable for spherical particles/nanoparticles and low particle volume fractions. Brinkman [41] presented the relationship between viscosity of solutions and suspensions of moderate particle as

$$\frac{\mu_{nf}}{\mu_{bf}}=\frac{1}{(1-\phi)^{2.5}}. \tag{25}$$

where μ_{bf} is known as viscosity of the base fluid, μ_{nf} is known as viscosity of the nanofluid and ϕ is known as particle volume fractions. Following Nguyen et al. [7], the correlation for computing the relative viscosity of 47nm Al_2O_3–Water nanofluid with higher particle volume fraction is

$$\frac{\mu_{nf}}{\mu_{bf}}=0.904e^{0.148\phi}. \tag{26}$$

Considering the experimental procedure of Nguyen et al. [7], Eq. (26) is reliable to investigate nanofluid flow for the case $0\%\leqslant\phi\leqslant 0.8\%$. Following Motsa et al. [42], the density of the nanofluid ρ_{nf}, the heat capacity of the 47nm alumina–water nanofluid $(\rho C_p)_{nf}$ and the effective heat capacity of the spherical 47nm nanoparticle $(\rho C_p)_{sp}$ are defined as

$$\rho_{nf}=(1-\phi)\rho_{bf}+\phi\rho_{sp},\ (\rho C_p)_{nf}=(1-\phi)(\rho C_p)_{bf}+\phi(\rho C_p)_{sp},$$
$$\alpha_{nf}=\frac{\kappa_{nf}}{(\rho C_p)_{nf}},\ \frac{\kappa_{nf}}{\kappa_{bf}}=\frac{\kappa_{sp}+2\kappa_{bf}-2\phi(\kappa_{bf}-\kappa_{sp})}{\kappa_{sp}+2\kappa_{bf}+\phi(\kappa_{bf}-\kappa_{sp})} \tag{27}$$

The thermo-physical properties of the base fluid (water) and different spherical nanoparticles by Oztop and Abu-Nada [43] is considered and presented in Table 1. Also, the volumetric coefficients of thermal expansion (β) and electrical conductivity of the nanofluid (σ) are treated as constant function of volume fraction.

Table 1 Thermo-physical properties of base fluid (water) and spherical 47nm alumina nanoparticles (Al_2O_3).

Physical properties	Base fluid (water)	Al_2O_3
C_p (J kg^{-1} K)	4179	765
ρ (kg/m^3)	997.1	3970
κ (W/mK)	0.613	40

2.4. Non-dimensionalization and parametrization

In order to non-dimensionalize and parameterize Eqs. (14), (15), (18), (19), (20) and (21) subject to boundary conditions Eqs. (22) and (23) we consider the following variables

$$\eta=y\left(\frac{m+1}{2}\frac{U_o}{\vartheta_{bf}}\right)^{1/2}(x+b)^{\frac{m-1}{2}},\ T_w(x)=A(x+b)^{\frac{1-m}{2}},$$
$$\theta=\frac{T-T_\infty}{T_w(x)-T_\infty},\ \frac{T}{T_\infty}=[1+\theta\theta_w-\theta]$$
$$\psi(x,y)=f\left(\frac{2}{m+1}\right)^{1/2}(\vartheta_{bf}U_o)^{1/2}(x+b)^{\frac{m+1}{2}},$$
$$m_m(\eta)=\frac{N-N_\infty}{N_w-N_\infty}\ g(\eta)=\frac{a}{a_o},\ h(\eta)=\frac{\ell}{a_o}. \tag{28}$$

The continuity equation is satisfied automatically. The dimensionless governing equation of the form

$$\frac{0.904e^{0.148\phi}}{(1-\phi)+\phi\frac{\rho_{sp}}{\rho_{bf}}}\frac{d^3f}{d\eta^3}-\frac{2m}{m+1}\frac{df}{d\eta}\frac{df}{d\eta}+f\frac{d^2f}{d\eta^2}$$
$$-\frac{\zeta}{1-\phi+\phi\frac{\rho_{sp}}{\rho_{bf}}}\left(\frac{2}{m+1}\right)\frac{df}{d\eta}+G_{rm}\theta=0, \tag{29}$$

$$\left(\frac{\frac{\kappa_{sp}+2\kappa_{bf}-2\phi(\kappa_{bf}-\kappa_{sp})}{\kappa_{sp}+2\kappa_{bf}+\phi(\kappa_{bf}-\kappa_{sp})}}{1-\phi+\phi\frac{(\rho C_p)_{sp}}{(\rho C_p)_{bf}}}+\frac{(1+\theta\theta_w-\theta)^3}{R\left[1-\phi+\phi\frac{(\rho C_p)_{sp}}{(\rho C_p)_{bf}}\right]}\right)\frac{d^2\theta}{d\eta^2}+N_b\frac{dg}{d\eta}\frac{d\theta}{d\eta}$$
$$+N_t\frac{d\theta}{d\eta}\frac{d\theta}{d\eta}-P_r\frac{1-m}{m+1}\frac{df}{d\eta}\theta+P_r f\frac{d\theta}{d\eta}$$
$$+3\frac{(1+\theta\theta_w-\theta)^2}{R\left[1-\phi+\phi\frac{(\rho C_p)_{sp}}{(\rho C_p)_{bf}}\right]}(\theta_w-1)\frac{d\theta}{d\eta}\frac{d\theta}{d\eta}$$
$$+P_r\gamma\frac{2}{m+1}\frac{Exp[-n\eta]}{\left[1-\phi+\phi\frac{(\rho C_p)_{sp}}{(\rho C_p)_{bf}}\right]}=0, \tag{30}$$

$$\frac{d^2g}{d\eta^2}+S_{ca}f\frac{dg}{d\eta}-S_{ca}K\frac{2}{m+1}gh^3-\frac{N_t}{N_b}\frac{d^2\theta}{d\eta^2}=0, \tag{31}$$

$$\delta\frac{d^2h}{d\eta^2}+S_{cb}f\frac{dh}{d\eta}+S_{cb}K\frac{2}{m+1}gh^3+\frac{N_t}{N_b}\frac{d^2\theta}{d\eta^2}=0, \tag{32}$$

$$\frac{d^2m_m}{d\eta^2}-S_{mm}\frac{1-m}{m+1}\frac{df}{d\eta}m_m+S_{mm}f\frac{dm_m}{d\eta}-m_mP_e\frac{d^2g}{d\eta^2}$$
$$-P_e\frac{dg}{d\eta}\frac{dm_m}{d\eta}=0. \tag{33}$$

In order to non-dimensionalize the boundary conditions, it is pertinent to note that the minimum value of y is not the starting point of the slot. This implies that all the conditions

in Eq. (22) are not imposed at $y = 0$. As shown in Fig. 1, it is obvious that it may not be realistic to say that $y = 0$ at all point on upper horizontal surface of paraboloid of revolution. Hence, not valid to set $y = 0$ in similarity variable η. Upon using $y = A(x+b)^{\frac{1-m}{2}}$ which is the starting point of the flow at the slot the minimum value of y accurately corresponds to minimum value of similarity variable η as

$$\eta = A\left(\frac{m+1}{2}\frac{U_o}{\vartheta}\right)^{1/2}$$

Let $\chi = A\left(\frac{m+1}{2}\frac{U_o}{\vartheta}\right)^{1/2}$. This implies that at the wall (i.e. on upper horizontal surface of paraboloid of revolution), the boundary condition suitable to scale the boundary layer flow is $\eta = \chi$. The boundary condition becomes

$$\frac{df}{d\chi} = 1,\ f(\chi) = \chi\frac{1-m}{m+1},\ \theta(\chi) = 1,\ \frac{dg}{d\chi} = \Lambda g(\chi),$$
$$\delta\frac{dh}{d\chi} = -\Lambda g(\chi),\ m_m(\chi) = 1,\ at\ \chi = \eta. \tag{34}$$

$$\frac{df}{d\chi} \to 0,\ \theta(\chi) \to 0,\ g(\chi) \to 1,\ h(\chi) \to 0,\ m_m(\chi) \to 0\ as\ \chi \to \infty. \tag{35}$$

In the dimensionless equation, ϕ is known as volume fraction, ρ_{sp} density of the spherical nanoparticles, ρ_{bf} density of base fluid (water), m is velocity power index (herein <1), G_{rm} is buoyancy induced parameter, κ_{nf} is the thermal conductivity of the nanofluid, κ_{bf} is the thermal conductivity of the base fluid, $(\rho C_p)_{sp}$ is known as the heat capacity of the nanoparticles, $(\rho C_p)_{bf}$ is known as the heat capacity of the base fluid, N_t is known as thermophoresis parameter, N_b is known as Brownian motion parameter, δ ratio of diffusion coefficients chemical reactant A to reactant B, θ_w is the temperature parameter, R is the radiation parameter, P_r is known as Prandtl number, γ is known as space dependent internal heat source parameter, n is the intensity of internal heat generation parameter, S_{ca} is the ratio of viscous diffusion rate to mass diffusion rate of reactant A, S_{cb} is the ratio of viscous diffusion rate to mass diffusion rate of specie B, K is known as strength of the homogeneous reaction, Λ is known as strength of the heterogeneous reaction, S_{mm} is the Schmidt number for diffusing motile microorganism, ζ is known as magnetic field parameter and P_e is known as the bioconvection Peclet number. All these parameters are defined as

$$G_{rm} = \frac{g\beta(T_w - T_\infty)}{U_o^2(x+b)^{2m-1}},\ \alpha_{nf} = \frac{\kappa_{nf}}{(\rho C_p)_{nf}},\ P_e = a_o\frac{c_h W_c}{\Delta a D_n},$$
$$\Lambda = \frac{K_s}{D_A\left(\frac{m+1}{2}\frac{U_o}{\vartheta_{bf}}\right)^{1/2}(x+b)^{\frac{m-1}{2}}}$$
$$\gamma = \frac{Q_o}{(\rho C_p)_{bf}U_o(x+b)^{m-1}},\ P_r = \frac{(\rho C_p)_{bf}\vartheta_{bf}}{\kappa^*} = \frac{\vartheta_{bf}}{\alpha_{bf}},$$
$$N_b = \frac{\tau D_A a_o}{\alpha_{nf}},\ N_t = \frac{\tau(T_w - T_\infty)}{\alpha_{nf}}\frac{D_T}{T_\infty},\ \theta_w = \frac{T_w}{T_\infty}$$
$$R = \frac{3k^*\kappa^*}{16\sigma^* T_\infty^3},\ S_{ca} = \frac{\vartheta_{bf}}{D_A},\ S_{cb} = \frac{\vartheta_{bf}}{D_B},\ K = \frac{K_1 a_o a_o^2}{U_o(x+b)^{m-1}},$$
$$\delta = \frac{D_B}{D_A},\ S_{mm} = \frac{\vartheta_{bf}}{D_n},\ \zeta = \frac{\sigma B_o^2}{U_o\rho_{bf}} \tag{36}$$

The dimensionless governing Eqs. (29)–(33) are depending on η while the boundary conditions Eqs. (34) and (35) are functions and/or derivatives depending on χ. In order to transform the domain from $[\chi,\infty)$ to $[0,\infty)$ it is valid to adopt $F(\varsigma) = F(\eta-\chi) = f(\eta)$, $\Theta(\varsigma) = \Theta(\eta-\chi) = \theta(\eta)$, $G(\varsigma) = G(\eta-\chi) = g(\eta)$, $H(\varsigma) = H(\eta-\chi) = h(\eta)$ and $M_m(\varsigma) = M_m(\eta-\chi) = m_m(\eta)$. The final dimensionless governing equations (coupled system of nonlinear ordinary differential equation) for spherical 47nm alumina–water nanofluid are

$$\frac{0.904e^{0.148\phi}}{1-\phi+\phi\frac{\rho_{sp}}{\rho_{bf}}}\frac{d^3F}{d\varsigma^3} - \frac{2m}{m+1}\frac{dF}{d\varsigma}\frac{dF}{d\varsigma} + F\frac{d^2F}{d\varsigma^2} - \frac{\zeta}{1-\phi+\phi\frac{\rho_{sp}}{\rho_{bf}}}\left(\frac{2}{m+1}\right)\frac{dF}{d\varsigma} + G_{rm}\Theta = 0, \tag{37}$$

$$\left(\frac{\frac{\kappa_{sp}+2\kappa_{bf}-2\phi(\kappa_{bf}-\kappa_{sp})}{\kappa_{sp}+2\kappa_{bf}+\phi(\kappa_{bf}-\kappa_{sp})}}{1-\phi+\phi\frac{(\rho C_p)_{sp}}{(\rho C_p)_{bf}}} + \frac{(1+\theta_w\Theta-\Theta)^3}{R\left[1-\phi+\phi\frac{(\rho C_p)_{sp}}{(\rho C_p)_{bf}}\right]}\right)\frac{d^2\Theta}{d\varsigma^2} + N_b\frac{dG}{d\varsigma}\frac{d\Theta}{d\varsigma} + N_t\frac{d\Theta}{d\varsigma}\frac{d\Theta}{d\varsigma} - P_r\frac{1-m}{m+1}\frac{dF}{d\varsigma}\Theta + P_rF\frac{d\Theta}{d\varsigma} + 3\frac{(1+\theta_w\Theta-\Theta)^2}{R\left[1-\phi+\phi\frac{(\rho C_p)_{sp}}{(\rho C_p)_{bf}}\right]}(\theta_w-1)\frac{d\Theta}{d\varsigma}\frac{d\Theta}{d\varsigma} + P_r\gamma\frac{2}{m+1}\frac{Exp[-n\varsigma]}{\left[1-\phi+\phi\frac{(\rho C_p)_{sp}}{(\rho C_p)_{bf}}\right]} = 0, \tag{38}$$

$$\frac{d^2G}{d\varsigma^2} + S_{ca}F\frac{dG}{d\varsigma} - S_{ca}K\frac{2}{m+1}GH^3 - \frac{N_t}{N_b}\frac{d^2\Theta}{d\varsigma^2} = 0, \tag{39}$$

$$\delta\frac{d^2H}{d\varsigma^2} + S_{cb}F\frac{dH}{d\varsigma} + S_{cb}K\frac{2}{m+1}GH^3 + \frac{N_t}{N_b}\frac{d^2\Theta}{d\varsigma^2} = 0, \tag{40}$$

$$\frac{d^2M_m}{d\varsigma^2} - S_{mm}\frac{1-m}{m+1}\frac{dF}{d\varsigma}M_m + S_{mm}F\frac{dM_m}{d\varsigma} - M_mP_e\frac{d^2G}{d\varsigma^2} - P_e\frac{dG}{d\varsigma}\frac{dM_m}{d\varsigma} = 0. \tag{41}$$

Subject to boundary conditions

$$\frac{dF}{d\varsigma} = 1,\ F(\varsigma) = \chi\frac{1-m}{m+1},\ \Theta(\varsigma) = 1,\ \frac{dG}{d\varsigma} = \Lambda g(\varsigma),$$
$$\delta\frac{dH}{d\varsigma} = -\Lambda G(\varsigma),\ M_m(\varsigma) = 1\ at\ \varsigma = 0. \tag{42}$$

$$\frac{dF}{d\varsigma} \to 0,\ \Theta(\varsigma) \to 0,\ G(\varsigma) \to 1,\ H(\varsigma) \to 0,$$
$$M_m(\varsigma) \to 0\ as\ \varsigma \to \infty. \tag{43}$$

The quantities of interest are the skin friction coefficient C_{fx}, Nusselt number Nu_x and density number of the motile microorganism Jn_x which are defined as

$$C_{fx} = \frac{\tau_w}{\rho_{bf}\sqrt{\frac{m+1}{2}}(U_w)^2},\ Nu_x = \frac{(x+b)q_w}{\kappa_{bf}[T_w(x)-T_\infty]\sqrt{\frac{m+1}{2}}},$$
$$Jn_x = \frac{(x+b)L_w}{D_n[N_w(x)-N_\infty]\sqrt{\frac{m+1}{2}}}.$$

where τ_w is the shear stress (skin friction) on the stretching sheet along the upper surface of horizontal paraboloid of rev-

olution, q_w is the heat flux from the sheet and L_w denotes the wall motile microorganisms flux

$$\tau_w = \left(\mu_{nf}\frac{\partial u}{\partial y}\bigg|_{y=A(x+b)^{\frac{1-m}{2}}},\ q_w = -\left(\kappa_{nf}+\frac{16\sigma^* T^3}{3k^*}\right)\frac{\partial T}{\partial y}\bigg|_{y=A(x+b)^{\frac{1-m}{2}}},\right.$$
$$\left. L_w = -\left(D_n\frac{\partial N}{\partial y}\bigg|_{y=A(x+b)^{\frac{1-m}{2}}}\right.\right.$$

Upon using the similarity variables in Eq. (28) we obtain

$$\frac{Re_x^{1/2}C_{fx}}{0.904e^{0.148\phi}} = F''(0),$$
$$Nu_x Re_x^{-1/2} = -\left(\frac{\kappa_{sp}+2\kappa_{bf}-2\phi(\kappa_{bf}-\kappa_{sp})}{\kappa_{sp}+2\kappa_{bf}+\phi(\kappa_{bf}-\kappa_{sp})}+\frac{(1+\Theta\theta_w-\Theta)^3}{R}\right)\Theta'(0),$$
$$Jn_x Re_x^{-1/2} = -M'_m(0),\ Re_x = \frac{U_w(x+b)}{\vartheta_{bf}} \tag{44}$$

where Re_x is the local Reynolds number.

3. Numerical solution

Numerical solutions of the ordinary differential Eqs. (37)–(41) subject to Neumann boundary conditions (42) and (43) are obtained using classical Runge–Kutta method with shooting techniques and MATLAB package (bvp5c). The boundary value problem cannot be solved on an infinite interval and it would be impractical to solve it for even a very large finite interval. In this study, the infinite boundary condition at a finite point ς is 7. The set of coupled nonlinear ordinary differential equations along with boundary conditions have been reduced to a system of eleven simultaneous equations of first order for eleven unknowns following the method of superposition in Na [44].

3.1. Classical Runge–Kutta method along with shooting techniques

In order to integrate the corresponding I.V.P., the values of $F''(\varsigma=0)$, $\Theta'(\varsigma=0)$, $G(\varsigma=0)$, $H(\varsigma=0)$ and $M'_m(\varsigma=0)$ are required. However, such values do not exist after the non-dimensionalization of the boundary conditions (22) and (23). Although, at specific value of δ and Λ the correct values for $G'(\varsigma=0)$ and $H'(\varsigma=0)$ can be easily obtained once $G(\varsigma=0)$ is known. The suitable guess values for $F''(\varsigma=0)$, $\Theta'(\varsigma=0)$, $G(\varsigma=0)$, $H(\varsigma=0)$ and $M'_m(\varsigma=0)$ are chosen and then numerical integration was carried out. The calculated values of $F'(\varsigma)$, $\Theta(\varsigma)$, $G(\varsigma)$, $H(\varsigma)$ and $M_m(\varsigma)$ at infinity ($\varsigma=7$) are compared with the given boundary conditions in Eq. (43) and the estimated values $F''(\varsigma=0)$, $\Theta'(\varsigma=0)$, $G(\varsigma=0)$, $H(\varsigma=0)$ and $M'_m(\varsigma=0)$ are adjusted to give a better approximation for the solution. Series of values for $F''(\varsigma=0)$, $\Theta'(\varsigma=0)$, $G(\varsigma=0)$, $H(\varsigma=0)$ and $M'_m(\varsigma=0)$ are considered and applied with fourth-order classical Runge–Kutta method using step size $\triangle\varsigma=0.01$. The above procedure is repeated until asymptotically converged results are obtained within a tolerance level of 10^{-4}. It is very important to remark that setting $\varsigma_\infty=7$, all profiles are compatible with the boundary layer theory and asymptotically satisfy the conditions at free stream as suggested by Pantokratoras [45]. It is worth mentioning that there exist no related published articles that could be used to validate the accuracy of the present numerical results. Meanwhile, Eqs. (37)–(41) subject to Neumann boundary conditions (42) and (43) can easily be solved using ODE solvers such as MATLAB's bvp5c.

3.2. MATLAB package (bvp5c)

The Matlab package (bvp5c) integrates a system of ordinary differential equations of the form $y'=f(x,y)$ on the interval $\varsigma\in[a,b]$ subject to two-point boundary value conditions $bc(y(a),y(b))=0$; see Gökhan [46]. The bvp5c is a finite difference code that implements the four-stage Lobatto IIIa formula. This is a collocation formula and the collocation polynomial provides a C^1-continuous solution that is fifth-order accurate uniformly in $\varsigma\in[a,b]$. The formula is implemented as an implicit Runge–Kutta formula. The bvp5c solves the algebraic equations directly while bvp4c uses analytical condensation. The bvp4c handles unknown parameters directly while bvp5c augments the system with trivial differential equations for unknown parameters; for details, see Kierzenka and Shampine [47]. The Matlab package (bvp5c) was chosen because in terms of scalar evaluation, the performance of bvp5c solver is better than bvp4c.

3.3. Verification of the results

In order to verify the accuracy of the present analysis, the results of classical Runge–Kutta together with shooting have been compared with that of bvp5c solution for the limiting case when $Pr=6.8$, $\zeta=0.4$, $S_{mm}=1.3$, $S_{ca}=0.62$, $S_{cb}=1.3$, $K=0.4$, $\gamma=0.09$, $n=0.4$, $m=0.4$, $N_b=0.2$, $\phi=0.2$, $\chi=0.4$, $\Lambda=0.4$, $G_{rm}=1$, $\delta=1.2$, $R=1$, $\theta_w=1.2$, $\rho_{sp}=3970$, $\rho_{bf}=997.1$, $\kappa_{sp}=40$, $\kappa_{bf}=0.613$, $(\rho Cp)_{sp}=3,037,050$, $(\rho Cp)_{bf}=4,166,880.9$, $P_e=0.2$ at various values of thermophoresis parameter N_t. As shown in Table 2, the comparison in the above case is found to be in good agreement. This good agreement is an encouragement for further study of the effects of other parameters on the flow of 47nm alumina–water nanofluid within boundary layer formed on upper horizontal surface of paraboloid of revolution.

Table 2 Comparison between the solutions of classical Runge–Kutta together with shooting (RK4SM) and MATLAB solver bvp5c for the limiting case.

N_t	$G(\varsigma=0)$ (RK4SM)	$H(\varsigma=0)$ RK4SM	$G(\varsigma=0)$ (bvp5c)	$H(\varsigma=0)$ (bvp5c)
0.2	−0.679861212281121	0.745939667410071	−0.679861212489451	0.745939667411087
0.4	−0.992609757667148	0.782682286599284	−0.992609752167983	0.782682286599968
0.6	−1.549357315176777	0.788606967447703	−1.549357317776777	0.788606967447728

4. Results and discussion

The numerical computations have been carried out for various values of volume fraction (ϕ), buoyancy induced parameter (G_{rm}) and thickness parameter (χ) in order to study its effects on the motion of spherical 47nm Al_2O_3–water nanofluid within boundary layer. The effects of these pertinent parameters on the velocity profiles $F'(\varsigma)$, temperature profiles $\Theta(\varsigma)$, temperature gradient profiles $\Theta'(\varsigma)$, concentration of reactant A (homogeneous-bulk fluid) $G(\varsigma)$, concentration gradient of reactant A $G'(\varsigma)$, concentration of reactant B (heterogeneous-catalyst at the surface) $H(\varsigma)$, concentration gradient of reactant B $H'(\varsigma)$ and diffusion of motile microorganism $Mm(\varsigma)$ within boundary layer flow of 47nm alumina–water nanofluid containing gyrotactic-microorganisms are illustrated. When $Pr = 6.8$, $\zeta = 0.4$, $S_{mm} = 1$, $S_{ca} = 0.62$, $S_{cb} = 1.3$, $K = 0.4$, $\gamma = 0.09$, $n = 0.4$, $m = 0.3$, $N_b = 0.2$, $N_t = 0.3$, $\chi = 0.4$, $\Lambda = 0.4$, $G_{rm} = 1$, $\delta = 1.2$, $R = 1$, $\theta_w = 1.2$, $\rho_{sp} = 3970$, $\rho_{bf} = 997.1$, $\kappa_{sp} = 40$, $\kappa_{bf} = 0.613$, $(\rho Cp)_{sp} = 3,037,050$, $(\rho Cp)_{bf} = 4,166,880.9$ and $P_e = 0.2$, effects of solid volume fraction of nanoparticles (ϕ) on vertical velocity and horizontal velocity profiles within boundary layer are illustrated in Figs. 2a, 2b, 2c, 2d. It is found that the velocity along x-direction and y-direction of two-dimensional alumina–water nanofluid containing 47nm spherical nanoparticles and gyrotactic-microorganisms increases as the magnitude of ϕ increases. Also, the increase in $F(\varsigma)$ and $F'(\varsigma)$ when ϕ ranges from 0.6 to 0.8 is highly substantial compared to when it ranges from 0.4 to 0.6. Practically speaking, as magnitude of ϕ increases this enhances the heat capacity of the nanofluid since it is a multiple of $(\kappa_{bf} - \kappa_{sp})$ and $(\rho C_p)_{sp}$; whereas $(\rho Cp)_{sp} = 3,037,050$ and $(\rho Cp)_{bf} = 4,166,880.9$. In fact, with the nature of increase observed in $\Theta(\varsigma)$ with ϕ boiling may occur for $\phi > 1.2$. As the nanofluid climbs the upper horizontal surface of paraboloid of revolution, it is noticed that shear stress increases near the wall; see Fig. 2c. This result implies that in the presence of stretching at the wall, temperature profile and concentration of homogeneous bulk fluid increase while concentration of heterogeneous catalyst at the surface decreases with volume fraction ϕ; see Figs. 2d, 2e, 2f. Fig. 3a and 3b illustrate the influence of buoyancy parameters on horizontal velocity profiles $F'(\varsigma)$ and temperature profiles $\Theta(\varsigma)$ of steady two dimensional 47nm alumina–water nanofluid flow along an upper horizontal surface of paraboloid of revolution in the presence of nonlinear thermal radiation (i.e. $R = 1$ and $\theta_w = 1.2$), Lorentz force (i.e. $\zeta = 0.4$) and higher value of

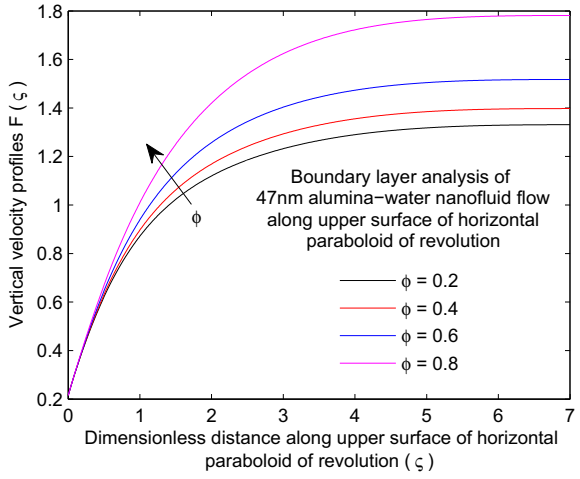

Figure 2a Effect of ϕ on $F(\varsigma)$.

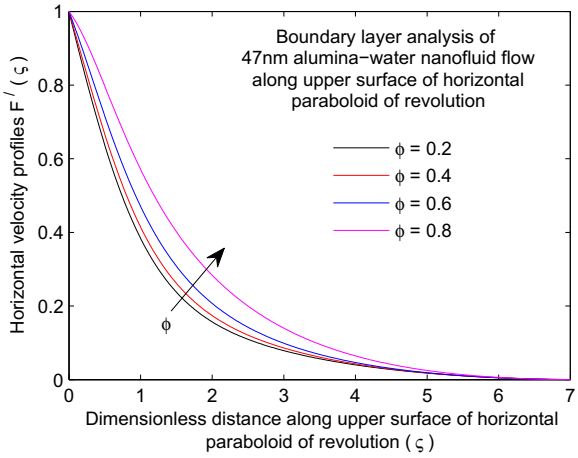

Figure 2b Effect of ϕ on $F'(\varsigma)$.

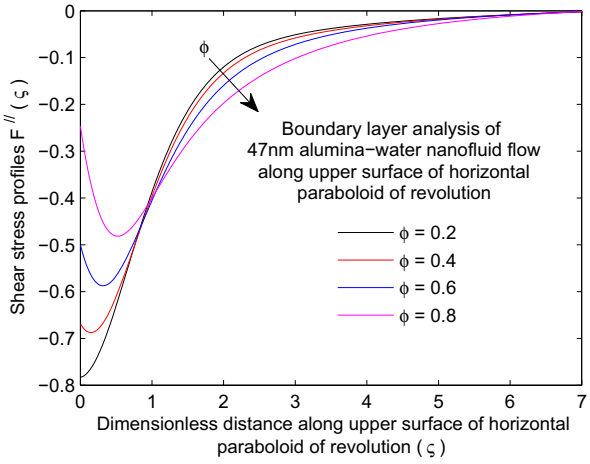

Figure 2c Effect of ϕ on $F''(\varsigma)$.

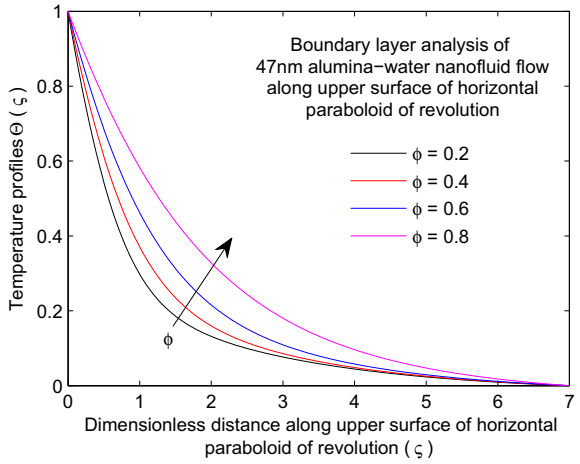

Figure 2d Effect of ϕ on $\Theta(\varsigma)$.

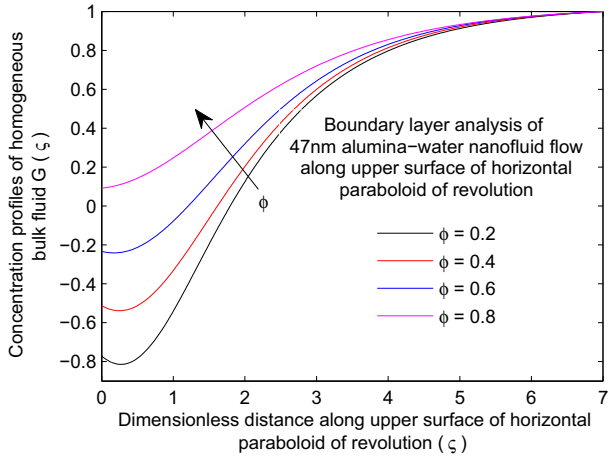

Figure 2e Effect of ϕ on $G(\varsigma)$.

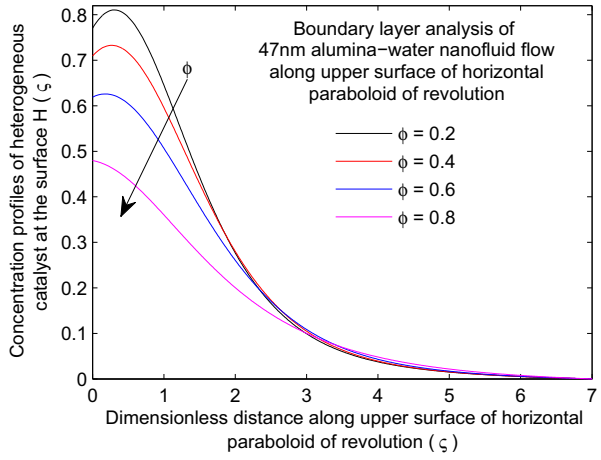

Figure 2f Effect of ϕ on $H(\varsigma)$.

volume fraction (i.e. $\phi = 0.8$) when $Pr = 6.8$, $S_{mm} = 1$, $S_{ca} = 0.62$, $S_{cb} = 1.3$, $K = 0.4$, $\gamma = 0.09$, $n = 0.4$, $m = 0.3$, $N_b = 0.2$, $N_t = 0.3$, $\chi = 0.4$, $\Lambda = 0.4$, $\delta = 1.2$, $\rho_{sp} = 3970$, $\rho_{bf} = 997.1$, $\kappa_{sp} = 40$, $\kappa_{bf} = 0.613$, $(\rho Cp)_{sp} = 3{,}037{,}050$, $(\rho Cp)_{bf} = 4{,}166{,}880.9$ and $P_e = 0.2$. It is observed that the horizontal velocity profiles increase while temperature profiles decrease with an increase in G_{rm}. Indeed, maximum velocity is obtained when $G_{rm} = 4$ near upper horizontal surface of paraboloid of revolution $0.2 \leqslant \varsigma \leqslant 0.6$. When nanofluid heats up, the molecules of both the base fluid and nanoparticles become excited and begins to move. The energy of this movement is enough to overcome the forces that bind the intermolecular forces together, allowing the fluid to move faster and decreasing its viscosity; hence, the velocity increases significantly. Moreover, as the magnitude of G_{rm} increases the tendency of 47nm alumina–water nanofluid to flow (i.e. climb) the surface is increased and hence boasts the velocity profiles. Since the base fluid is water, the 47nm alumina particles absorb the heat energy which is generated by the variation in density due to temperature; this accounts for the decrease in temperature with G_{rm}. It is very important to remark that this result is in good agreement with that of Vedavathi et al. [48].

It is further observed that buoyancy parameter has negligible effect on $G(\varsigma)$ and $H(\varsigma)$ near the wall. Within the fluid

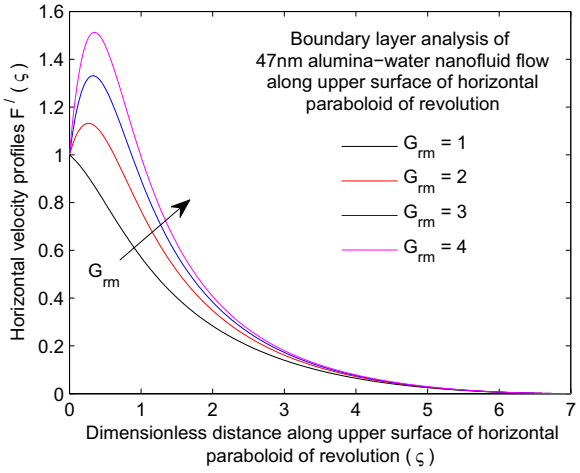

Figure 3a Effect of G_{rm} on $F'(\varsigma)$.

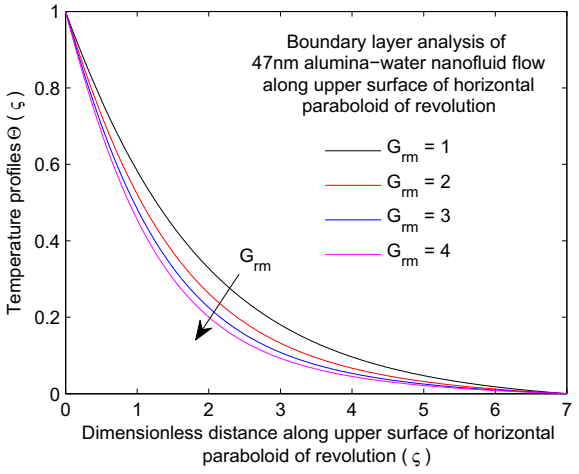

Figure 3b Effect of G_{rm} on $\Theta(\varsigma)$.

domain (i.e. few layers of the fluid on the horizontal surface of paraboloid of revolution), it is seen that at maximum value of G_{rm} the concentration of homogeneous bulk fluid is found to be maximum while concentration of heterogeneous catalyst at the surface is found to be minimum; see Figs. 3c and 3d. However, it is further noticed that diffusion of motile microorganism $M_m(\varsigma)$ is a decreasing function of buoyancy parameter G_{rm}; see Fig. 3e. One of the major attributes of paraboloid of revolution is thickness parameter (χ). This quantifies the thickness of the horizontal surface with non-uniform thickness. An attempt has been made to investigate the effect of thickness parameter χ and the results are illustrated in Figs. 4a, 4b, 4c, 4d, 4e, 4f, 4g, 4h and 4i. When buoyancy parameter $G_{rm} = 3$, it is observed that vertical velocity $F(\varsigma)$ increases equally with χ at all points in the domain ($0 \leqslant \varsigma \leq 7$) while the horizontal velocity $F'(\varsigma)$ is a decreasing function of χ. This result is in good agreement with Fig. 6 reported by Anjali Devi and Prakash [26]; it was stated that increase in wall thickness parameter acts as the retarding factor for the velocity distribution. Physically, large values of thickness parameter correspond to the object which is very thick; hence, the motion along such object will be very slow. In addition, it is observed in Fig. 4c

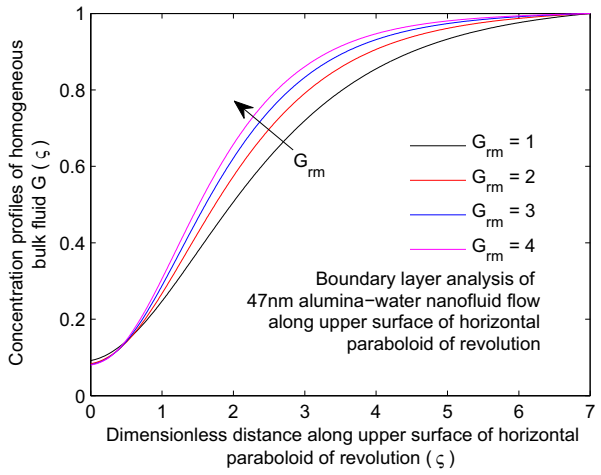

Figure 3c Effect of G_{rm} on $G(\varsigma)$.

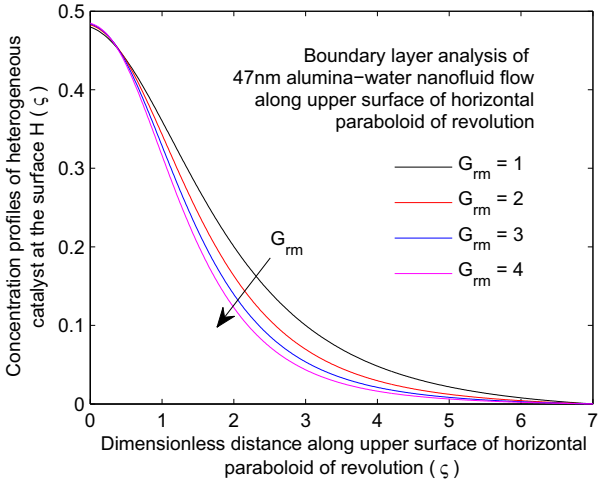

Figure 3d Effect of G_{rm} on $H(\varsigma)$.

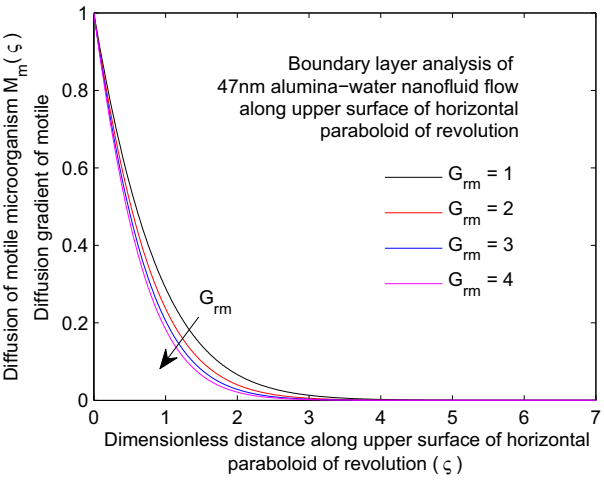

Figure 3e Effect of G_{rm} on $M_m(\varsigma)$.

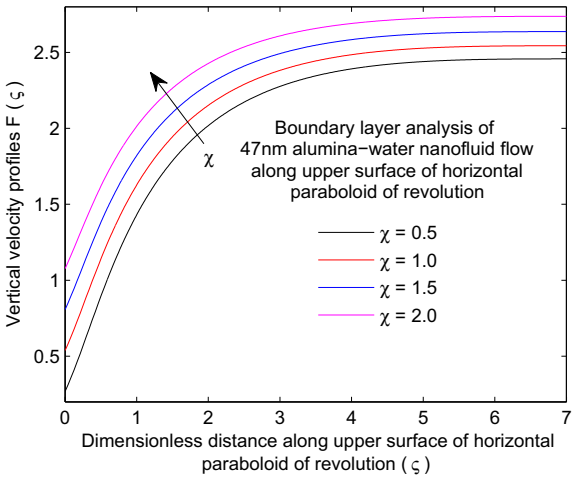

Figure 4a Effect of χ on $F(\varsigma)$.

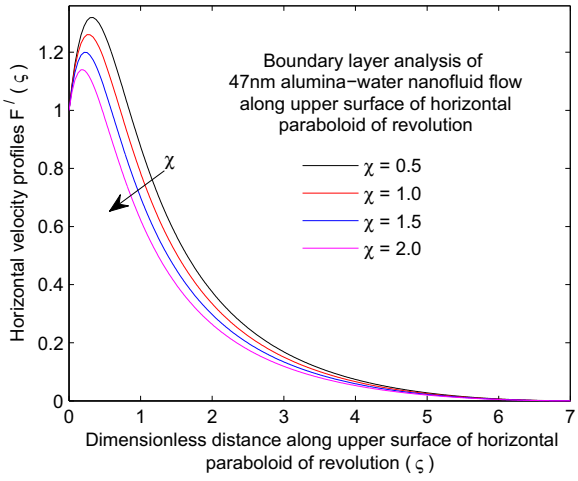

Figure 4b Effect of χ on $F'(\varsigma)$.

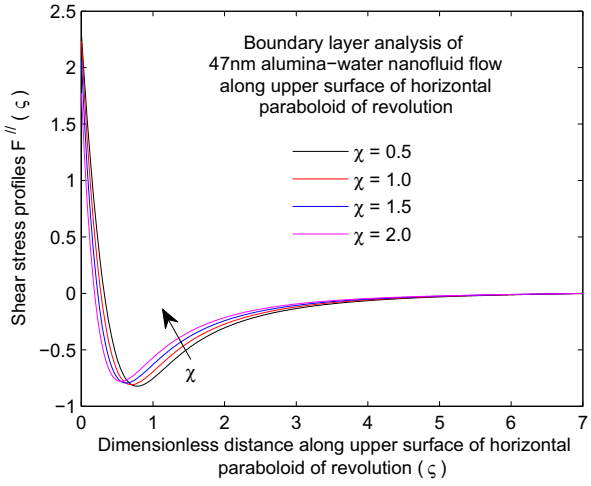

Figure 4c Effect of χ on $F''(\varsigma)$.

that the shear stress decreases with χ near the surface and thereafter increases with χ within the fluid domain. From Fig. 4d it can be deduced that temperature is a decreasing function of thickness parameter. Practically, as magnitude of χ increases, the thickness of paraboloid of revolution increases and hence more heat energy is needed to induce the flow.

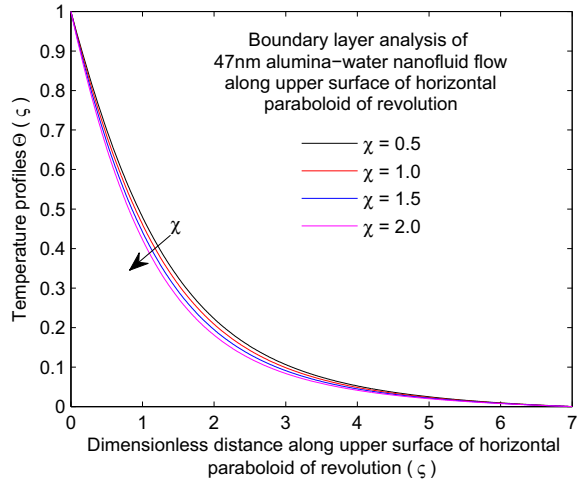

Figure 4d Effect of χ on $\Theta(\varsigma)$.

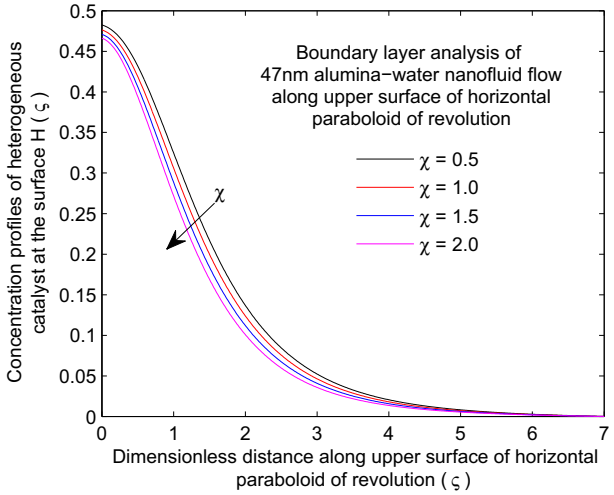

Figure 4g Effect of χ on $H(\varsigma)$.

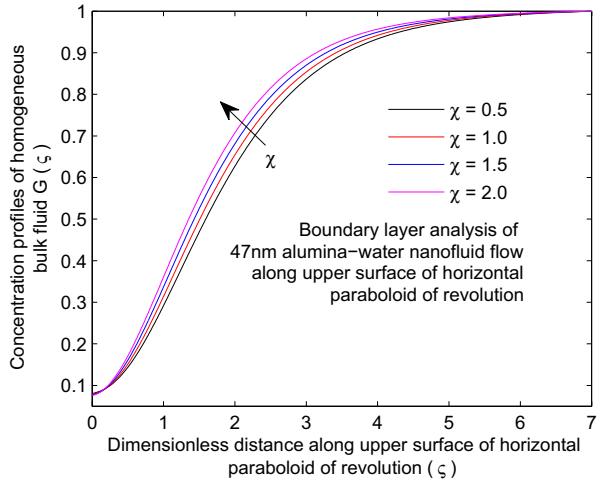

Figure 4e Effect of χ on $G(\varsigma)$.

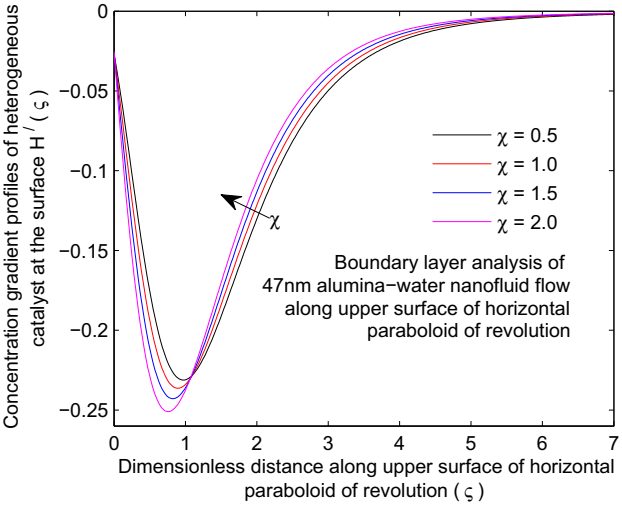

Figure 4h Effect of χ on $H'(\varsigma)$.

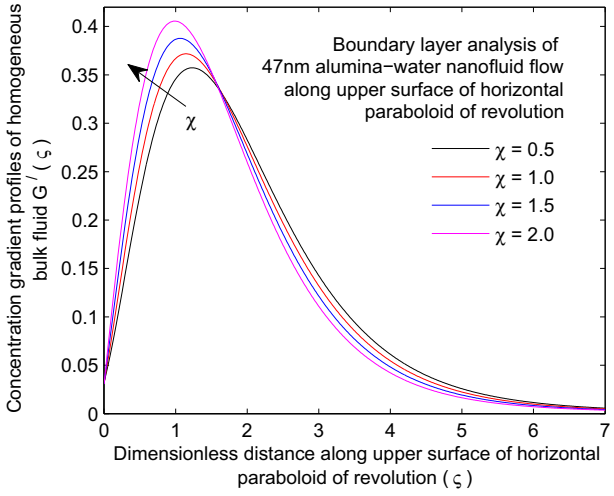

Figure 4f Effect of χ on $G'(\varsigma)$.

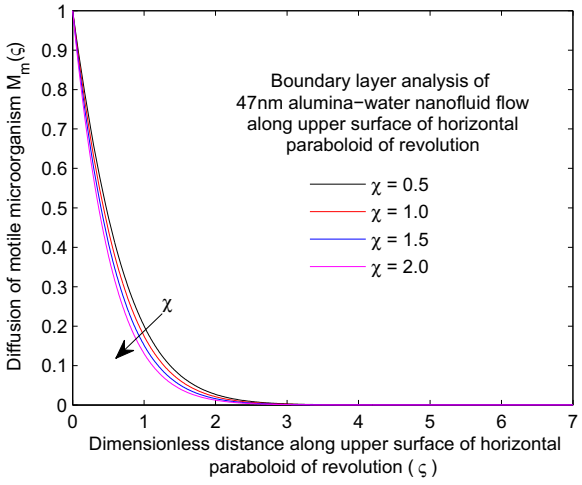

Figure 4i Effect of χ on $M_m(\varsigma)$.

Table 3 Effect of m on $F''(0), -\Theta(0)$ and $-M_m(0)$ when $\phi = 0.2$, $Pr = 6.8$, $\zeta = 0.4$, $S_{mm} = 1$, $S_{ca} = 0.62$, $S_{cb} = 1.3$, $K = 0.4$, $\gamma = 0.09$, $n = 0.4$, $N_b = 0.2$, $N_t = 0.3$, $\chi = 0.4$, $\Lambda = 0.4$, $G_{rm} = 1$, $\delta = 1.2$, $R = 1$, $\theta_w = 1.2$, $\rho_{sp} = 3970$, $\rho_{bf} = 997.1$, $\kappa_{sp} = 40$, $\kappa_{bf} = 0.613$, $(\rho Cp)_{sp} = 3,037,050$, $(\rho Cp)_{bf} = 4,166,880.9$ and $P_e = 0.2$.

m	$\frac{Re_x^{1/2}C_f}{0.904e^{0.148\phi}}$	$\frac{Nu_x Re_x^{-1/2}}{\left(\frac{\kappa_{sp}+2\kappa_{bf}-2\phi(\kappa_{bf}-\kappa_{sp})}{\kappa_{sp}+2\kappa_{bf}+\phi(\kappa_{bf}-\kappa_{sp})}+\frac{(1+\Theta\theta_w-\Theta)^3}{R}\right)}$	$Jn_x Re_x^{-1/2}$
0.1	−0.807879010530699	1.355081672552685	1.249679002044798
0.2	−0.794010243255343	1.232581728332564	1.146513389708621
0.3	−0.783254738682585	1.125941083723210	1.056149146833120
0.4	−0.774614832279268	1.032079381681961	0.976165196379606
0.5	−0.767465521005872	0.948675865166087	0.904729719379674

Scientifically, this effect may be controlled and influenced by increasing or decreasing internal heat source parameter. This explains the decrease in the temperature profiles as illustrated in Fig. 4d. With an increase in the magnitude of χ, the concentration of bulk fluid increases while the concentration of catalyst at the surface decreases within the fluid domain as shown in Figs. 4e and 4g. At fixed strength of the homogeneous reaction ($K = 0.4$), strength of the heterogeneous reaction ($\Lambda = 0.4$) and ratio of diffusion coefficients chemical reactant A to reactant B ($\delta = 1.2$), it is observed that $G'(\varsigma)$ increases while $H'(\varsigma)$ decreases near the surface; see Fig. 4f and 4h. Also, it is discovered in Fig. 4i that diffusion of motile microorganism $M_m(\varsigma)$ decreases with an increase in χ. Table 3 presents the effect of velocity index parameter m on local skin friction coefficients $F''(0)$, local Nusselt number $-\Theta(0)$ and density number of motile microorganism at the wall $-M_m(0)$. It is observed that with an increase in the magnitude of m, local skin friction coefficients along the wall of paraboloid of revolution increase while local Nusselt number which is proportional to heat transfer rate decreases. In addition, the density number of the motile microorganism at the wall is found to be decreasing with an increase in the magnitude of m.

5. Conclusion

The present study reports the boundary layer analysis of two-dimensional 47nm alumina–water nanofluid flow along an upper horizontal surface of paraboloid of revolution in the presence of nonlinear thermal radiation and Lorentz force. Quartic autocatalysis kind of homogeneous heterogeneous chemical reaction and governing equation suitable to unravel the thermophoresis which takes place in the boundary layer are presented. The proposed modified buoyancy-induced model for the case of convective flow ($m < 1$) is suitable enough to investigate boundary layer formed on upper horizontal surface of paraboloid of revolution (where $T_w(x) > T_\infty$). At large value of volume fraction ϕ the heat capacity and other properties of 47nm alumina–water nanofluid greatly generate more heat energy which account for the overshoot in velocity and temperature functions. Larger values of thickness parameter (χ) correspond to higher concentration of the homogeneous bulk fluid and lower concentration of heterogeneous catalyst. It can also be concluded that increase in velocity index parameter m corresponds to an increase in local skin friction coefficient and decrease in local Nusselt number.

Acknowledgments

The author would like to thank anonymous reviewers for their valuable comments and useful suggestions. Contributions of Professor Andrey V. Kuznetsov, Professor Oluwole D. Makinde and Professor Asterios Pantokratoras to the body of knowledge on bioconvection, convective heat transfer and boundary layer theory are highly appreciated.

References

[1] E.J. Davis, Thermophoresis of Particles, Encyclopedia of Surface and Colloid Science, Online version of Taylor & Francis, 2006, http://dx.doi.org/10.1081/E-ESCS-120000614, pp. 6274–6282.
[2] L. Talbot, R.K. Cheng, R.W. Scheffer, D.P. Wills, Thermophoresis of particles in a heated boundary layer, J. Fluid Mech. 101 (1980) 737–758.
[3] R. Tsai, Y.P. Chang, T.Y. Lin, Combined effects of thermophoresis and electrophoresis on particle deposition onto a Wafer, J. Aerosol Sci. 29 (1998) 811–825.
[4] I.L. Animasaun, Dynamics of unsteady MHD convective flow with thermophoresis of particles and variable thermo-physical properties past a vertical surface moving through binary mixture, Open J. Fluid Dyn. 5 (2015) 106–120, http://dx.doi.org/10.4236/ojfd.2015.52013.
[5] N. Sandeep, C. Sulochana, C.S.K. Raju, M.J. Babu, V. Sugunamma, Unsteady boundary layer flow of thermophoretic MHD nanofluid past a stretching sheet with space and time dependent internal heat source/sink, Appl. Appl. Math. 10 (2015) 312–327.
[6] S.U.S. Choi, Enhancing thermal conductivity of fluids with nanoparticles, Proceedings of the ASME International Mechanical Engineering Congress and Exposition, San Francisco, Calif, USA, vol. 66, 1995, pp. 99–105.
[7] H.A. Mintsa, C.T. Nguyen, G. Roy, New temperature dependent thermal conductivity data of water based nanofluids, Proceedings of the 5th IASME/WSEAS Int. Conference on Heat Transfer, Thermal Engineering and Environment, Athens, Greece, vol. 290, 2007, pp. 25–27.
[8] N. Sandeep, C. Sulochana, I.L. Animasaun, Stagnation-point flow of a Jeffrey nano fluid over a stretching surface with induced magnetic field and chemical reaction, Int. J. Eng. Res. Africa 20 (2016) 93–111, http://dx.doi.org/10.4028/www.scientific.net/JERA.20.93.
[9] J.R. Platt, "Bioconvection patterns" in cultures of free-swimming organisms, Science 133 (1961) 1766–1767.
[10] S. Ghorai, N.A. Hill, Wavelengths of gyrotactic plumes in bioconvection, Bull. Math. Biol. 62 (2000) 429–450.

[11] A.V. Kuznetsov, A.A. Avramenko, Effect of small particles on the stability of bioconvection in a suspension of gyrotactic microorganisms in a layer of finite depth, Int. Commun. Heat Mass Transfer 31 (2004) 1–10.
[12] W.A. Khan, O.D. Makinde, MHD nanofluid bioconvection due to gyrotactic microorganisms over a convectively heat stretching sheet, Int. J. Therm. Sci. 81 (2014) 118–124, http://dx.doi.org/10.1016/j.ijthermalsci.2014.03.009.
[13] A. Malvandi, S.A. Moshizi, D.D. Ganji, Two-component heterogeneous mixed convection of alumina/water nanofluid in microchannels with heat source/sink, Adv. Powder Technol. 27 (2016) 245–254.
[14] S.A. Moshizi, Forced convection heat and mass transfer of MHD nanofluid flow inside a porous microchannel with chemical reaction on the walls, Eng. Comput. 32 (2015) 2419–2442.
[15] A. Malvandi, S.A. Moshizi, D.D. Ganji, Nanofluids flow in microchannels in presence of heat source/sink and asymmetric heating, J. Thermophys. Heat Transfer 30 (2016) 111–119.
[16] A. Malvandi, S.A. Moshizi, D.D. Ganji, Effect of magnetic fields on heat convection inside a concentric annulus filled with Al_2O_3–water nanofluid, Adv. Powder Technol. 25 (2014) 1817–1824.
[17] A. Malvandi, S.A. Moshizi, D.D. Ganji, An analytical study on unsteady motion of vertically falling spherical particles in quiescent power-law shear-thinning fluids, J. Mole. Liq. 193 (2014) 166–173.
[18] A. Raees, X.U. Hang, S.U.N. Qiang, I. Pop, Mixed convection in gravity-driven nano-liquid film containing both nanoparticles and gyrotactic microorganisms, Appl. Math. Mech. 36 (2015) 163–178, http://dx.doi.org/10.1007/s10483-015-1901-7 (English Edition).
[19] I.L. Animasaun, Effects of thermophoresis, variable viscosity and thermal conductivity on free convective heat and mass transfer of non-darcian MHD dissipative Casson fluid flow with suction and *n*th order of chemical reaction, J. Nigerian Math. Soc. 34 (2015) 11–31, http://dx.doi.org/10.1016/j.jnnms.2014.10.008.
[20] M.A. Chaudhary, J.H. Merkin, A simple isothermal model for homogeneous–heterogeneous reactions in boundary-layer flow. I. Equal diffusivities, Fluid Dyn. Res. 16 (1995) 311–333.
[21] S.K. Scott, Isolas, mushrooms and oscillations in isothermal, autocatalytic reaction–diffusion equations, Chem. Eng. Sci. 42 (1987) 307–315.
[22] R. Nandkeolyar, S.S. Motsa, P. Sibanda, Viscous and joule heating in the stagnation point nanofluid flow through a stretching sheet with homogenous–heterogeneous reactions and nonlinear convection, J. Nanotechnol. Eng. Med. 4 (2013), http://dx.doi.org/10.1115/1.4027435, 041001-1.
[23] I.L. Animasaun, C.S.K. Raju, N. Sandeep, Unequal diffusivities case of homogeneous–heterogeneous reactions within viscoelastic fluid flow in the presence of induced magnetic-field and nonlinear thermal radiation, Alex. Eng. J. 55 (2) (2016) 1595–1606.
[24] L.L. Lee, Boundary layer over a thin Needle, Phys. Fluids 10 (1967) 820, http://dx.doi.org/10.1063/1.1762194.
[25] R.T. Davis, M.J. Werle, Numerical solutions for laminar incompressible flow past a paraboloid of revolution, Am. Inst. Aeronaut. Astronaut. J. 10 (1972) 1224–1230.
[26] S.P. Anjali Devi, M. Prakash, Temperature dependent viscosity and thermal conductivity effects on hydromagnetic flow over a slendering stretching sheet, J. Nigerian Math. Soc. (2015) (in press). doi:http://dx.doi.org/10.1016/j.jnnms.2015.07.002.
[27] T. Fang, J. Zhang, Y. Zhong, Boundary layer flow over a stretching sheet with variable thickness, Appl. Math. Comput. 218 (2015) 7241–7252.
[28] A.V. Kuznetsov, D.A. Nield, Natural convective boundary layer flow of a nanofluid past a vertical plate, Int. J. Therm. Sci. 49 (2010) 243–247.
[29] A.V. Kuznetsov, D.A. Nield, Double-diffusive natural convective boundary layer flow of a nanofluid past a vertical plate, Int. J. Therm. Sci. 50 (2011) 712e717, http://dx.doi.org/10.1016/j.ijthermalsci.2011.01.003.
[30] D.T. Lynch, Chaotic behavior of reaction systems: mixed cubic and quadratic autocatalysis, Chem. Eng. Sci. 47 (1992) 4435–4444.
[31] T.J. Pedle, N.A. Hill, J.O. Kessler, The growth of bioconvection patterns in a uniform suspension of gyrotactic micro-organisms, J. Fluid Mech. 195 (1988) 223–338.
[32] A.V. Kuznetsov, The onset of nanofluid bioconvection in a suspension containing both nanoparticles and gyrotactic microorganisms, Int. Commun. Heat Mass Transfer 37 (2010) 1421–1425.
[33] J. Boussinesq, Theorie de l'ecoulement tourbillonnant et tumultueux des liquides dans les lits rectilignes a grande section, Gauthier-Villars Paris vol. 1, Open Library OL7070543M, 1897.
[34] A.O. Oyem, I.L. Animasaun, Effect of variable viscosity, dufour, soret and thermal conductivity on free convective heat and mass transfer of non-Darcian flow past porous flat surface, Am. J. Comput. Math. 4 (2014) 357–365, http://dx.doi.org/10.4236/ajcm.2014.44030.
[35] F. Shahraki, Modeling of buoyancy-driven flow and heat transfer for air in a horizontal annulus: effects of vertical eccentricity and temperature-dependent properties, Numer. Heat Transfer, Part A: Appl.: Int. J. Comput. Methodol. 42 (2002) 603–621, http://dx.doi.org/10.1080/10407780290059729.
[36] J.I. Diaz, J.M. Rakotoson, P.G. Schmidt, A parabolic system involving a quadratic gradient term related to the Boussinesq approximation, Rev. Real Acad. Ciencias Ser. A Mat. 101 (2007) 113–118.
[37] I.L. Animasaun, Double diffusive unsteady convective micropolar flow past a vertical porous plate moving through binary mixture using modified Boussinesq approximation, Ain Shams Eng. J. (2015) (in press). doi:http://dx.doi.org/10.1016/j.asej.2015.06.010.
[38] S. Rosseland, Astrophysik aud Atom-Theoretische Grundlagen, Springer, Berlin, 1931, pp. 41–44.
[39] I.L. Animasaun, Casson fluid flow of variable viscosity and thermal conductivity along exponentially stretching sheet embedded in a thermally stratified medium with exponentially heat generation, J. Heat Mass Transfer Res. 3 (2016) (in press).
[40] VYa Rudyak, Viscosity of nanofluids – why it is not described by the classical theories, Adv. Nanoparticles 2 (2013) 266–279, http://dx.doi.org/10.4236/anp.2013.23037.
[41] H.C. Brinkman, The viscosity of concentrated suspensions and solutions, J. Chem. Phys. 20 (1952) 571, http://dx.doi.org/10.1063/1.1700493.
[42] S.S. Motsa, N.A. Haroun, P. Sibanda, S. Mondal, On unsteady MHD mixed convection in a nanofluid due to a stretching/shrinking surface with suction/injection using the spectral relaxation method, Bound. Value Probl. 24 (2015) (in press). doi:http://dx.doi.org/10.1186/s13661-015-0289-5.
[43] H. Oztop, E. Abu-Nada, Numerical study of natural convection in partially heated rectangular enclosures filled with nanofluids, Int. J. Heat Fluid Flow 29 (2008) 1326–1336.
[44] T.Y. Na, Computational Methods in Engineering Boundary Value Problems, Academic Press, New York, 1979.
[45] A. Pantokratoras, A common error made in investigation of boundary layer flows, Appl. Math. Model. 33 (2009) 413–422.

[46] F.S. Gökhan, Effect of the Guess Function & Continuation Method on the Run Time of MATLAB BVP Solvers, Clara M. Ionescu (Ed.), 2011, p. 1.
[47] J. Kierzenka, L.F. Shampine, A BVP solver based on residual control and the MATLAB PSE, ACM TOMS 27 (3) (2001) 299–316.
[48] N. Vedavathi, K. Ramakrishna, K.J. Reddy, Radiation and mass transfer effects on unsteady MHD convective flow past an infinite vertical plate with Dufour and Soret effects, Ain Shams Eng. J. 6 (2015) 363–371, http://dx.doi.org/10.1016/j.asej.2014.09.009.